



1 Brief communication: Atmospheric moisture and near-surface 2 temperature anomalies: key drivers in the 2022 European mega- 3 drought

4 José C. Fernández-Alvarez^{1,2,3*}, Raquel Nieto^{2,4,5}, Sergio M. Vicente-Serrano⁶, David Carvalho³, Luis
5 Gimeno^{2,4,5}

8 ¹Galicia Supercomputing Center (CESGA), Climate System Research Unit, Santiago de Compostela, 15705, Spain

9 ²Centro de Investigación Mariña, Universidade de Vigo, Environmental Physics Laboratory (EPhysLab), Campus As Lagoas
10 s/n, Ourense, 32004, Spain

11 ³CESAM, Departamento de Física, Universidade de Aveiro, 3810-193, Aveiro, Portugal.

12 ⁴Climate System Research Unit, UVigo-CESGA, Ourense, 32004, Spain

13 ⁵Unidad Asociada CSIC-Universidad de Vigo: Grupo de Física de la Atmósfera y del Océano, Ourense, Spain

14 ⁶Instituto Pirenaico de Ecología, Consejo Superior de Investigaciones Científicas (IPE-CSIC), Zaragoza, Spain

15

16 Correspondence to: José C. Fernández-Alvarez (jcffernandez@cesga.es)

17 **Abstract.** Using a Lagrangian framework, we show that the 2022 European drought was driven by a sharp
18 reduction in precipitation contributions from Atlantic and Mediterranean moisture sources, despite enhanced
19 atmospheric moisture uptake. Persistent anticyclonic circulation suppressed convection and diverted moisture
20 away from Europe. Lagrangian temperature-source decomposition reveals strong adiabatic warming as the
21 dominant heat driver. Together, weakened oceanic moisture supply and subsidence-driven warming sustained and
22 intensified the drought.

23 1 Main

24 Europe experienced an exceptional drought in 2022, resulting in widespread agricultural losses (Baruth, B. et al.,
25 2022; Toreti et al., 2022; Faranda et al., 2023), reductions in hydropower and wind energy, increased solar
26 potential (Toreti et al., 2022; Copernicus, 2022a), disruptions to river transport and ecosystems, severe water
27 shortages, forest fires, and substantial anomalies in carbon emissions (Toreti et al., 2022; Faranda et al., 2023;
28 Copernicus, 2022b; Gharun et al., 2024).

29 Previous analyses have investigated the event's drivers and its links to anthropogenic climate change, showing
30 that it produced the largest terrestrial water storage deficit since 2002 across Central–Southern Europe, with
31 human-induced warming amplifying drought intensity by more than 30% (Bevacqua et al., 2024). The drought



32 was primarily driven by a persistent anticyclonic anomaly, which, together with other large-scale atmospheric
33 circulation features —a blocking over western Europe and a displaced jet stream— extreme heat, and elevated
34 atmospheric evaporative demand, exacerbated its severity (Faranda et al., 2023; Garrido-Pérez et al., 2024).
35 Easterly and southerly dry winds associated with the strengthened anticyclone further reinforced these conditions
36 (Herrera-Lormendez et al., 2023). However, although this drought is extraordinary in the context of the current
37 climate, soil droughts on a similar scale are projected to occur twice as often in west-central Europe in a +2 °C
38 warming (Schumacher et al., 2024).

39 While previous studies have elucidated the large-scale circulation and climate change influence, the specific role
40 of anomalous moisture and temperature sources in shaping the drought's evolution remains unclear. Here, we
41 addressed this gap by quantifying the anomalous sources of atmospheric moisture uptake and temperature during
42 the 2022 European drought, providing new insights into the coupled thermodynamic and dynamic processes
43 governing the origin and development of extreme droughts in Europe.

44 The 2022 drought affected extensive areas across both the Atlantic and Mediterranean climatic regions of Europe
45 (Fig. S1, fourth column). To analyse the event, we defined the drought-affected area using the 6-month
46 Standardized Precipitation Evapotranspiration Index (SPEI6) for June-August 2022 ("Supplementary Methods").
47 This area was then divided into two subregions based on their dominant oceanic moisture sources (Fig. 1a) as
48 indicated in Gimeno-Sotelo et al. (2024): the North-Atlantic-influenced region, covering northern and western
49 Europe (hereafter NW_Europe), and the Mediterranean-influenced region, encompassing southern and eastern
50 Europe (SE_Europe).

51 Monthly anomalies for key meteorological variables related to drought occurrence (Fig. 1b-h) illustrate the
52 temporal evolution across both European subregions. Persistent deficits in precipitation (Fig. 1b) and soil
53 moisture (Fig. 1e) emerge across both regions, particularly during May-August —the peak period, as shown
54 SPEI6 (Fig. 1c)— consistent with water storage deficits reported for central-southern Europe (Bevacqua et al.,
55 2024), while atmospheric evaporative demand increases (Fig. 1d), especially over NW_Europe. Suppression of
56 vertical motion and persistence of high-pressure systems sustained the drought conditions. Vertical velocity
57 anomalies at 500 hPa (Fig. 1f) indicate reduced upward motions except for September (the drought-breaking
58 month) and November 2022. Persistent anticyclonic conditions and blocking activity (Faranda et al., 2023;
59 Garrido-Pérez et al., 2024) are further evidenced by positive geopotential height anomalies at 850 hPa (Fig. 1g).



60 This stable circulation favoured strong and widespread surface warming across both regions (Fig. 1h), more
61 pronounced over NW_Europe during summer (~ 2.2 K), reflecting thermal persistence. These results highlight
62 spatio-temporal differences between the subregions, driven by coupled land–atmosphere processes, evidenced by
63 coherent anomalies in precipitation, soil moisture, evapotranspiration, temperature, and atmospheric stability
64 (Figs. S1–S3).

65 At a large scale, and complementary to land–atmosphere interactions, the moisture flux patterns (measured as
66 vertically integrated water vapour transport (IVT) anomalies, Fig. S4) also reveal circulation patterns modulating
67 the event. While the subtropical Atlantic exhibited positive IVT anomalies, western Europe experienced moisture
68 deficits before drought peak. The reduced inflow from the Mediterranean Sea limited replenishment of
69 atmospheric moisture and intensified the drought (with partial recovery from September), acting as a drought-
70 intensifying factor (Gimeno-Sotelo et al., 2024).

71 The role of changes in atmospheric moisture transport from source regions modulating droughts is recognized as
72 a key factor in understanding their behaviour and intensity (Gimeno et al., 2012; Liu et al., 2020). To quantify
73 this effect during the 2022 European drought, we applied a Lagrangian approach using the FLEXPART model
74 (Pisso et al., 2019) and ERA5 reanalysis data (Hersbach et al., 2020). This framework (“Supplementary
75 Methods”) enabled us to track the moisture feeding the two European subregions (moisture uptake, MU) and to
76 quantify the anomalous contribution to precipitation (PC) from the two main moisture sources, NATL and MED
77 (Gimeno-Sotelo et al., 2024; Gimeno et al., 2012), and from both European subregions themselves (Fig. S5).

78 Marked temporal and spatial contrasts emerged between NW_Europe and SE_Europe in the evolution of MU and
79 PC anomalies (Fig. 1i–p). From January to April, moisture availability preceding the peak drought was slightly
80 enhanced, as both subregions exhibited positive MU anomalies mainly from local sources (Fig. 1i–l). In contrast,
81 notable deficits in precipitation contributions (PC) occurred from MED and NATL sources, particularly from the
82 latter, while PC values from the subregions themselves remained close to climatology (Figs. 1m–o). On average,
83 anomalies during this period were markedly negative, ranging from -0.4 to -0.8 mm day $^{-1}$ for both dominant
84 oceanic sources (Fig. 2p).

85 From May to August (the drought peak), MU intensified from multiple sources, with a slight decrease from the
86 Mediterranean during some months. This coincides with predominantly negative PC anomalies, particularly from
87 NATL—although less pronounced than in preceding months (Fig. S3). During this period, mean moisture support



88 anomalies from MED and NATL were about -0.2 mm day^{-1} (Fig. 2p). These patterns are coherent with reduced
89 moisture flux and persistently stable atmospheric conditions associated with a sustained blocking pattern (Figs.
90 1f,g; Fig. S3) over the North Atlantic and Europe (Faranda et al., 2023; Garrido-Pérez et al., 2024).

91 During September to November, land-based sources became dominant for SE_Europe, while oceanic sources
92 prevailed for NW_Europe (Fig. 1i-l). Positive PC anomalies, mainly from the two European subregions and the
93 Mediterranean, indicate partial hydrological recovery, most evident in SE_Europe (Fig. 2p). In contrast, negative
94 PC anomalies from the NATL were marked but weaker than those before the drought peak. Overall, MU
95 increased, despite some declines south of 30°N (Fig. S6), reflecting the atmosphere's greater capacity to retain
96 moisture under higher temperatures (Soden and Held, 2006; Allen and Ingram; 2002) (Fig. 1h). However, PC
97 behaviour associated with the MED and NATL oceanic sources and the two European subregions suggests that,
98 although moisture availability increased, atmospheric instability required for convection and precipitation was
99 largely absent until September, consistent with stable conditions driven by persistent high-pressure systems
100 (Faranda et al., 2023; Garrido-Pérez et al., 2024), which inhibited upward motion and convection and diverted
101 moisture fluxes away from the preferred sources (positive omega500 and Z850 anomalies, and reduced IVT; Fig.
102 1f,g; Fig. S4). In general, weakening oceanic contributions to precipitation were key to sustaining the 2022
103 drought, which began to disappear by the late-season reactivation of regional moisture inputs (Figs. S7, S8).
104 Specifically, in September, drought across southern Europe ended abruptly as intense rainfall was triggered by a
105 deep North Atlantic trough extending into central Europe and a strong subtropical high over North Africa (Figs.
106 1m,n; S3). This pattern advected warm, moist Mediterranean air toward southeastern Europe (Fig. S8), initiating
107 severe convection under unstable conditions (Figs. 1f,g; Z850 and omega500 negative anomalies). This shift
108 marked the end of the prolonged dry period.

109

110

111

112

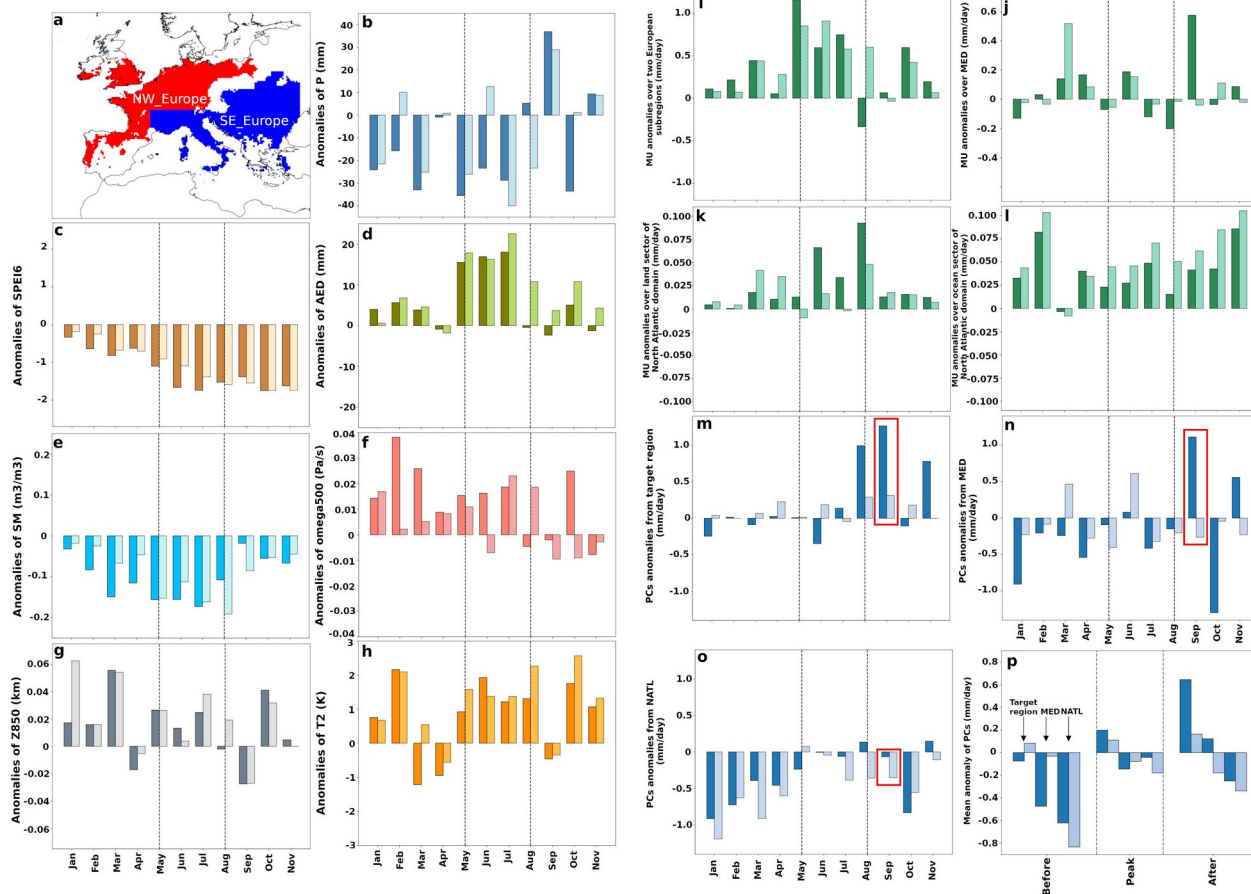
113

114



115

116



117

118

119

120

121

122

123

124

125

126

127

128

129

130

131

132

133

134

135

136

137

138

139

140

141

Fig. 1 Two European subregions, hydro-climatic monthly anomalies, moisture uptake (MU) and precipitation contributions (PCs) associated with the 2022 European drought | (a) Two European subregions considered in this study: northern-western Europe (NW_Europe, red) and southern-eastern Europe (SE_Europe, blue). (b-h) Monthly averaged anomalies of key hydro-climatic variables, calculated relative to the 1994–2023 climatology using ERA5 reanalysis data: (b), accumulated precipitation (P, mm), (c) 6-month Standardized Precipitation–Evapotranspiration Index (SPEI6), (d) atmospheric evaporative demand (AED, mm), (e) soil moisture (SM, m3/m3), (f) vertical velocity at 500 hPa (omega500, Pa/s), (g) geopotential height at 850 hPa (Z850, km), and (h) 2-meter temperature (T2, K) for both regions. (i-l) MU monthly anomalies (in mm/day, green plots) computed over: (i) each European subregion, (j) the Mediterranean Sea, from (k) land and (l) ocean sectors of the North Atlantic domain. (m-o) Monthly anomalies of PCs (mm/day, blue bars) from: (n) the Mediterranean (MED) moisture source, (o) the NATL, and (m) the two European subregions. (p) Average PCs



142 anomaly for each source for the period Before (January-April), the Peak of the drought (May-August) and After
143 (September-November). FLEXPART outputs forced ERA5 data has been used to determine MU and PCs. The
144 red rectangle indicates the month considered the drought-breaking month, September 2023. The period
145 considered for the calculation of the anomalies of the variables is 1994-2023, and the spatial patterns and
146 corresponding anomalies used to determine the monthly anomaly series are shown in Figs. S1-S3 and S6-S8.
147 Colour intensity indicates each region: higher intensity for SE_Europe and lower intensity for NW_Europe. The
148 framed area indicates the drought peak period (May–August 2022).

149 The 2022 European drought was additionally characterized by a considerable near-surface temperature excess
150 (Fig. 1h), accompanying several heatwaves (Schumacher et al., 2024). This thermal anomaly, linked to persistent
151 stable atmospheric conditions (Faranda et al., 2023; Garrido-Pérez et al., 2024), was a key factor in exacerbating
152 drought severity (Bevacqua et al., 2024). Using the Lagrangian framework (Papritz and Röhlisberger, 2023)
153 (“Supplementary Methods”), temperature anomaly sources for the two drought-affected European regions were
154 decomposed into adiabatic, diabatic, and advective components (Fig. 2), allowing identification of physical
155 drivers arising from vertical motion, horizontal transport, and heat exchange.

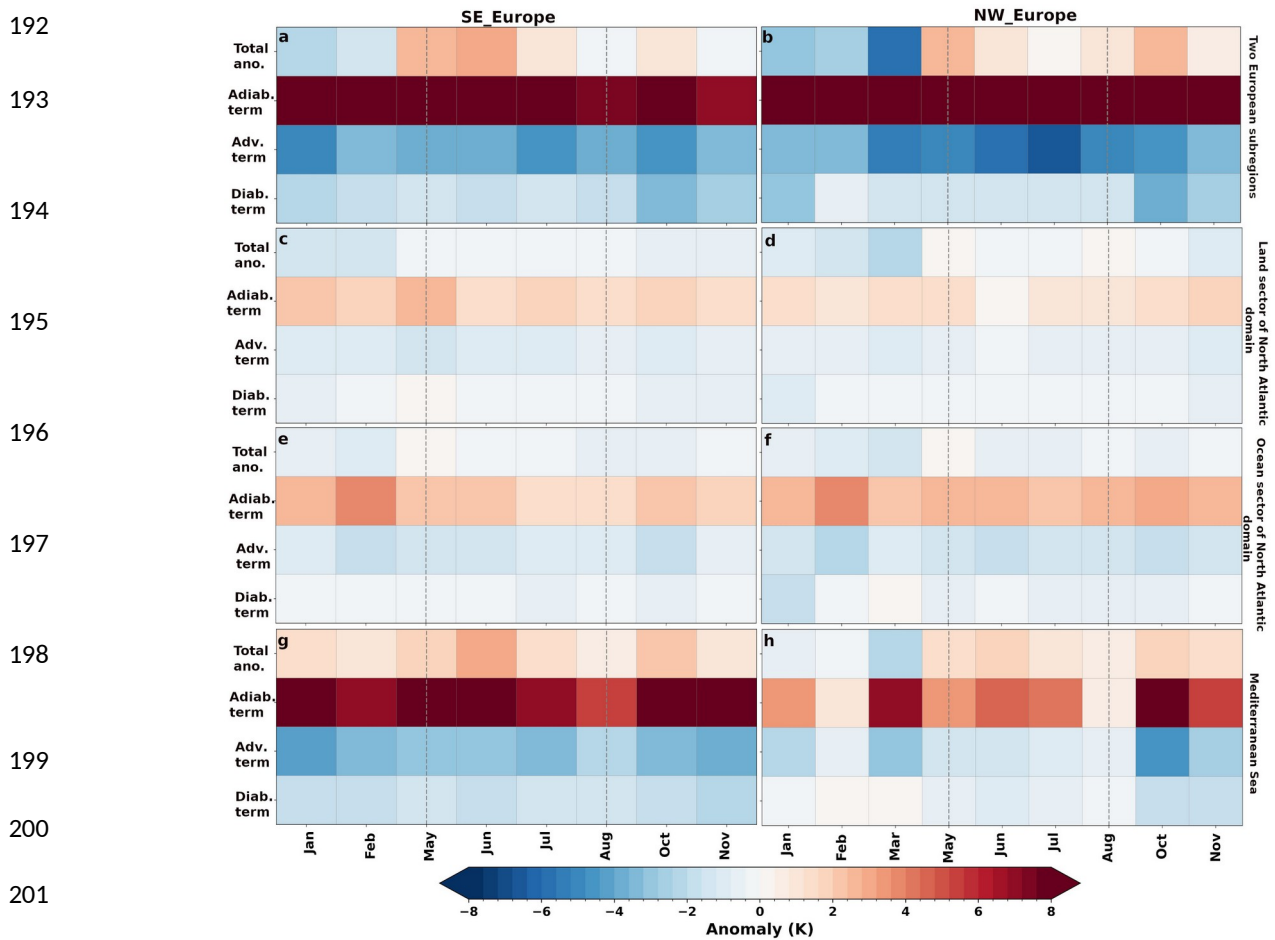
156 The two European subregions exhibit a dipolar pattern of total temperature anomaly sources, with positive
157 anomalies over North Africa, the Mediterranean region, the North Atlantic Ocean, and central-eastern Europe,
158 and negative anomalies north of 50° N. This pattern was strongest at the drought peak and expanded spatially
159 during January–February and May (Figs. S9, S10). Averages for the two European subregions reveal distinct
160 temporal and regional behaviours (Fig. 2). Over both subregions (Figs. 2a–b), the adiabatic term dominates year-
161 round, with pronounced positive values during the main drought period (May–August), indicating persistent
162 warming driven by subsidence and adiabatic compression. The advective term generally exhibits negative
163 anomalies during these same months, due to air flux from cooler higher latitudes, which partially offset the
164 adiabatic warming. The diabatic term also remains negative. Over the North Atlantic land and oceanic source
165 regions (Figs. 2c–f), anomalies are generally weaker than over the two European subregions, with modest
166 positive adiabatic and slightly negative diabatic and advective components, indicating minor remote contributions
167 to surface warming for the two European subregions. In contrast, over the Mediterranean Sea, strong positive
168 adiabatic anomalies occur (Figs. 2g–h), particularly during May–August and autumn, reflecting intense
169 subsidence. These periods correspond to the strongest total temperature anomalies, particularly in SE_Europe. A
170 percentage-based perspective (Figure S11) indicates that temperature anomalies for both European regions are
171 largely controlled by the continental regions themselves, explaining ~60–85% of the total signal, while the



172 Mediterranean Sea accounts for only ~10–30%. For the adiabatic term, European subregions contribute ~40–
173 60%, with Mediterranean influence near ~10–20%. A similar pattern is seen in the advective term, especially over
174 NW_Europe, where the European subregions explain between 40–60% of the anomalies. The diabatic term is
175 comparatively stronger over the Mediterranean (~20–40%), although the continental effects from the European
176 subregions still dominate (~50–70%).

177 The dominant adiabatic term is the fingerprint of a persistent anticyclonic circulation pattern (Faranda et al.,
178 2023; Garrido-Pérez et al., 2024), which results in descending air (Figs. S9, S10), confirming the major role of
179 adiabatic processes in controlling European temperature anomalies driven by summer anticyclones and mid-
180 tropospheric subsidence (Röhlisberger and Papritz, 2023; Hamal and Pfahl, 2024). The negative advective term
181 over the two European subregions reflects anticyclonic circulation moving air from cooler northeastern Europe
182 into the warmer European subregions (Figs. S9, S10).

183 The global cooling observed over the two subregions, linked to the diabatic term, is the result of the
184 compensation of three processes with different net effects on the temperature: (i) The warming by enhanced
185 evaporation (which occurs mainly over the ocean) resulting in enhanced condensation in the air with latent heat
186 absorption during the liquid-to-vapour phase transition and the cooling for inhibited evaporative (Röhlisberger
187 and Papritz, 2023) over central European land areas, due to reduced soil moisture (Bevacqua et al., 2024) (Figs.
188 S12, S13), resulting in diminished condensation in the air (ii) the warming by upward transfer of sensible heat
189 from the surface to the atmosphere, (Fig. S14), and (iii) the cooling by the imbalance in surface net longwave
190 radiation, under predominantly clear-sky and stable atmospheric conditions, as indicated by positive anomalies in
191 outgoing longwave radiation (Fig. S14); being the cooling processes dominant over the warming ones.



203 **Fig. 2 Monthly series of temperature anomaly sources during the 2022 European drought |**
 204 Heat maps show monthly anomalies of total temperature, and of the adiabatic, diabatic and advective
 205 components from January to November 2022. Left and right panels display anomalies for the SE_Europe and
 206 NW_Europe subregions, respectively. Panels show the anomaly values averaged over (a, b) each of the two
 207 European subregions, (c, d) the North Atlantic land sector, (e, f) the North Atlantic oceanic sector, and (g, h) the
 208 Mediterranean Sea. The framed period highlights the peak drought months (May–August 2022). Anomalies are
 209 computed relative to the 1994–2023 climatology. Data processed from FLEXPART outputs forced ERA5 data.

210 **2 Summary and Conclusions**



211 Our results show that the driving force behind the 2022 European mega-drought was not a lack of atmospheric
212 moisture, but persistent atmospheric stability that prevented moisture from becoming rainfall. A long-lasting
213 anticyclonic pattern blocked convection, diverted humid Atlantic and Mediterranean inflows, and triggered
214 widespread adiabatic warming that locked the region into deep dryness. The drought was therefore sustained by
215 descending air, warming-driven drying of the soil, and muted oceanic contributions. Its abrupt termination
216 highlighted the system's sensitivity: a shift toward unstable synoptic conditions was enough to reactivate regional
217 moisture sources and break the drought. These findings demonstrate that, in a warming climate, the severity of
218 future European droughts will depend not only on moisture availability but on the large-scale dynamics
219 controlling when and where rainfall can occur.

220 **Data and code availability**

221 ERA5 reanalysis is available via Copernicus Climate Data Store
222 (<https://cds.climate.copernicus.eu/cdsapp#!/dataset/reanalysis-era5-single-levels-monthly-means?tab=form>). FLEXPART
223 simulations can be generated following Vázquez et al. (2024). TROVA package is openly hosted on GitHub
224 (<https://github.com/tramo-ephyslab/TROVA-master> and the routines for decomposing temperature anomalies can be
225 retrieved from ETH Zurich Research Collection (<https://www.research-collection.ethz.ch/handle/20.500.11850/571107>).

226 **Author contributions**

227 J.C.F-A, L.G. and R.N. designed the study; J.C.F-A. performed the computation processing and obtaining the results; J.C.F-
228 A., L.G., R.N. S.V-S analysed the results; J.C.F-A., R.N., S.V-S., D.C. and L.G. wrote the paper; J.C.F-A., R.N., S.V-S.,
229 D.C. and L.G. review the paper.

230 **Competing interests**

231 The authors declare no competing interests.

232 **Acknowledgements**

233 J.C.F.-A. thanks the support from the Xunta de Galicia (Consellería de Cultura, Educación e Universidade) under the
234 Postdoctoral grant IN606B2024/016. David Carvalho acknowledges the FCT (Portuguese Foundation for Science and
235 Technology) and the Ministry of Science, Technology and Higher Education (MCTES) for his researcher contract



236 (CEECINST/00013/2021/CP2779/CT0017). This work has also been possible thanks to the computing resources and
237 technical support provided by CESGA (Centro de Supercomputación de Galicia) and the Red Española de
238 Supercomputación (RES) (DATA-2022-1-0001, DATA-2022-1-0003, DATA-2021-1-0005). The authors also acknowledge
239 the computer resources at Storage5 and the technical support provided by BSC (RES-DATA-2024-1-0002 and AECT-2025-
240 2-0048).

241 **Financial support**

242 EPhysLab members are supported by the SETESTRELO, ESMORGA, and APALPADOR projects (grants PID2021-
243 122314OB-I00, TED2021-129152B-C43, and PID2024-155515NB-I00) funded by the Ministerio de Ciencia, Innovación y
244 Universidades, Spain (MCIN/10.13039/501100011033), and the Xunta de Galicia (grant ED431C2021/44; Programa de
245 Consolidación e Estructuración de Unidades de Investigación Competitivas, Grupos de Referencia Competitiva). The
246 authors acknowledge FCT for the financial support to CESAM (UIDP/50017/2020, UIDB/50017/2020 & LA/P/0094/2020).
247 This work has also been supported by the research projects TED2021-129152B-C41 and PID2022-137244OB-I00, financed
248 by the Spanish Ministry of Science and FEDER, and by the MEHYDRO project (LINKB20080) funded by the i-LINK 2021
249 programme (CSIC), the CSIC Interdisciplinary Thematic Platform Clima (PTI-Clima), and the CSC2023-02-00 contract
250 financed by MITECO and the European Commission NextGenerationEU (Regulation EU 2020/2094). Additional support
251 was provided by the Unidad Asociada CSIC–Universidade de Vigo: Grupo de Física de la Atmósfera y del Océano.

252 **References**

253 Baruth, B. et al. JRC MARS Bulletin - Crop monitoring in Europe - September 2022 Vol. 30 No 9, in Van Den Berg, M. et
254 al. (eds.) Publications Office of the European Union, Luxembourg (2022). <https://doi.org/10.2760/067974>.

255 Toreti, A._et al. Drought in Europe July 2022, EUR 31147 EN, Publications Office of the European Union, Luxembourg
256 (2022). ISBN 978-92-76-54953-6, <https://doi.org/10.2760/014884>.

257 Faranda, D., Pascale, S. and Bulut, B.: Persistent anticyclonic conditions and climate change exacerbated the exceptional
258 2022 European-Mediterranean drought. Environ. Res. Lett. 18, 034030 (2023).

259 Copernicus Climate Change Service European State of the Climate 2022. Copernicus Climate Change Service (2022a).
260 Available at: <https://climate.copernicus.eu/esotc/2022> (Accessed: [March 16, 2025]).



261 Copernicus Climate Change Service European State of the Climate 2022: Drought (2022b). Available at:
262 <https://climate.copernicus.eu/esotc/2022> (Accessed: [March 16, 2025]).

263 Gharun, M., Shekhar, A., Xiao, J., Li, X., and Buchmann, N.: Effect of the 2022 summer drought across forest types in
264 Europe. *Biogeosciences*, 21, 5481–5494 (2024).

265 Bevacqua, E., Rakovec, O., Schumacher, D.L. et al.: Direct and lagged climate change effects intensified the 2022 European
266 drought. *Nat. Geosci.* 17, 1100–1107, <https://doi.org/10.1038/s41561-024-01559-2>. (2024)

267 Garrido-Pérez, J. M., Vicente-Serrano, S. M., Barriopedro, D., García-Herrera, R., Trigo, R., and Beguería, S.: Examining
268 the outstanding Euro-Mediterranean drought of 2021–2022 and its historical context. *J. of Hydrol.* 630, 130653.
269 <https://doi.org/10.1016/j.jhydrol.2024.130653>. (2024)

270 Herrera-Lormendez, P. et al.: European Summer Synoptic Circulations and Their Observed 2022 and Projected Influence on
271 Hot Extremes and Dry Spells. *Geophys. Res. Lett.* 10, e2023GL104580. <https://doi.org/10.1029/2023GL1>. (2023)

272 Schumacher, D. L. et al.: Detecting the human fingerprint in the summer 2022 Western–Central European soil drought.
273 *Earth Syst. Dyn.* 15, 131–154 (2024).

274 Gimeno-Sotelo, L., Fernández-Alvarez, J.C., Nieto, R. et al.: The increasing influence of atmospheric moisture transport on
275 hydrometeorological extremes in the Euromediterranean region with global warming. *Commun Earth Environ* 5, 604.
276 <https://doi.org/10.1038/s43247-024-01787-9>. (2024)

277 Gimeno, L. et al.: Oceanic and Terrestrial Sources of Continental Precipitation. *Rev. Geophysics* 50, RG4003 (2012).

278 Liu, B. et al. Global atmospheric moisture transport associated with precipitation extremes: Mechanisms and climate change
279 impacts. *WIREs Water* 7, e1412 (2020).

280 Pisso, I., et al.: The Lagrangian particle dispersion model FLEXPART version 10.4. *Geosci. Model Dev.* 12, 4955–4997
281 (2019).

282 Hersbach, H., Bell, B., Berrisford, P., Hirahara, S., Horányi, A., Muñoz-Sabater, J., et al.: The ERA5 global reanalysis. *Q. J.*
283 *R. Meteorol. Soc.*, 146, 1999–2049 (2020).

284 Soden, B. J., Held, I. M.: An assessment of climate feedbacks in coupled ocean-atmosphere models. *J. Clim.* 19, 6263–3360
285 (2006).

286 Allen, M. R., Ingram, W. J.: Constraints on future changes in climate and the hydrologic cycle. *Nature* 419, 228–232 (2002).



287 Papritz, L.; Röthlisberger, M.: A novel temperature anomaly source diagnostic: method and application to the 2021 heatwave
288 in the Pacific Northwest. *Geophys. Res. Lett.*, 50 (23), e2023GL105641 (2023).

289 Röthlisberger, M., Papritz, L.: Quantifying the physical processes leading to atmospheric hot extremes at a global scale. *Nat.*
290 *Geosci.* 16, 210–216 (2023).

291 Hamal, K., Pfahl, S. (2024).: Physical Processes Leading to Extreme day-to-day Temperatures Changes, Part I: Present-day
292 Climate. EGUsphere, 1-32 (2024).

293 Vázquez, M., Alvarez-Socorro, G., Fernández-Alvarez, J. C., Nieto, R., & Gimeno, L.: Global FLEXPART-ERA5
294 simulations using 30 million atmospheric parcels since 1980. *Zenodo*. <https://doi.org/10.5281/zenodo.12204017> (2024).